Microbial sphingomyelinase induces RhoA-mediated reorganization of the apical brush border membrane and is protective against invasion

David E. Saslowsky[a,b,c,†,*], Jay R. Thiagarajah[a,b,c,†], Beth A. McCormick[b,d], Jean C. Lee[c,e], and Wayne I. Lencer[a,b,c]

[a]Division of Gastroenterology and Nutrition and [b]Harvard Digestive Diseases Center, Boston Children's Hospital, Boston, MA 02115; [c]Harvard Medical School, Boston, MA 02115; [d]Department of Microbiology and Physiological Systems, University of Massachusetts Medical School, Worcester, MA 01655; [e]Division of Infectious Diseases, Department of Medicine, Brigham and Women's Hospital, Boston, MA 02115

ABSTRACT **The apical brush border membrane (BBM) of intestinal epithelial cells forms a highly structured and dynamic environmental interface that serves to regulate cellular physiology and block invasion by intestinal microbes and their products. How the BBM dynamically responds to pathogenic and commensal bacterial signals can define intestinal homeostasis and immune function. We previously found that in model intestinal epithelium, the conversion of apical membrane sphingomyelin to ceramide by exogenous bacterial sphingomyelinase (SMase) protected against the endocytosis and toxicity of cholera toxin. Here we elucidate a mechanism of action by showing that SMase induces a dramatic, reversible, RhoA-dependent alteration of the apical cortical F-actin network. Accumulation of apical membrane ceramide is necessary and sufficient to induce the actin phenotype, and this coincides with altered membrane structure and augmented innate immune function as evidenced by resistance to invasion by *Salmonella*.**

Monitoring Editor
Robert G. Parton
University of Queensland

Received: May 18, 2015
Revised: Jan 27, 2016
Accepted: Feb 1, 2016

INTRODUCTION

Sphingolipids are major components of eukaryotic cell membranes that play critical roles in membrane organization and function. Sphingomyelin (SM), by far the most abundant sphingolipid in mammalian cells, is particularly enriched in the brush border membrane (BBM) of intestinal epithelial cells (Simons and van Meer, 1988). It is concentrated in the outer leaflet of the plasma membrane (PM) and coalesces with cholesterol and other membrane components to form small, highly dynamic nanodomains often termed lipid rafts (Simons and Ikonen, 1997). SM-enriched lipid nanodomains have been implicated in the regulation of diverse membrane processes, including the initiation of signal transduction, cytoskeletal–membrane attachment, endocytosis, and vesicular trafficking (Lingwood and Simons, 2010), although the molecular basis for these functions is not fully understood.

Membrane nanodomains (lipid rafts) are linked both structurally and functionally to the actin cytoskeleton (Villalba *et al.*, 2001; Pelkmans *et al.*, 2002; Gowrishankar *et al.*, 2015), which contributes to the formation and maintenance of several key structures defining the apical pole of polarized enterocytes. This is the membrane surface that interfaces with the gut lumenal environment, and the actin cytoskeleton regulates in particular the apical microvilli and the perijunctional actin ring, which affect transcellular and paracellular intestinal permeability, respectively (Bretscher, 1991). To do this, the cortical F-actin underlying the BBM interacts dynamically with membrane anchor proteins. These assemblies are regulated in turn by membrane lipids and diverse protein effectors. At other sites, the

This article was published online ahead of print in MBoC in Press (http://www.molbiolcell.org/cgi/doi/10.1091/mbc.E15-05-0293) on February 10, 2016.

†These authors contributed equally.

*Address correspondence to: David Saslowsky (david.saslowsky@nih.gov).

Abbreviations used: BBM, brush border membrane; CT, cholera toxin; CTB, cholera toxin B-subunit; ERM, ezrin/radixin/moesin; SM, sphingomyelin; SMase, sphingomyelinase; TcdA, *Clostridium difficile* toxin A; TER, transepithelial resistance; TJ, tight junction.

cortical actin cytoskeleton is involved in many processes, including macropinocytosis, endocytosis, and cell migration. Many intestinal microbes and microbial products coopt the actin cytoskeleton for internalization into host cells, including *Salmonella*, *Listeria*, enterohemorrhagic *Escherichia coli* (EHEC), Shiga toxin, and cholera toxin (CT; Knutton *et al.*, 1989; Tilney and Portnoy, 1989; Finlay *et al.*, 1991; Badizadegan *et al.*, 2004; Romer *et al.*, 2010).

Sphingomyelinases (SMases) are enzymes that cleave the phosphorylcholine head group from SM, leaving the ceramide component intact in the cell membrane (Gulbins *et al.*, 2004). This alters membrane structure and function and can result in coalescence of ceramide-rich nanodomains (Grassme *et al.*, 2003). Membrane ceramide can also serve as a second messenger in signaling pathways affecting cellular differentiation, proliferation, apoptosis, cytokine production, and ion transport (Hannun, 1994; Gulbins *et al.*, 1997; Lepple-Wienhues *et al.*, 1999; Chik *et al.*, 2001; Ito *et al.*, 2004; Chapman *et al.*, 2005; Saslowsky *et al.*, 2009), thereby placing SMases as potential regulators of these pathways. Both commensal and pathogenic microbes that colonize the gastrointestinal tract can synthesize and secrete SMase (*Helicobacter pylori*, *Staphylococcus aureus* [also called β-hemolysin; Clarke *et al.*, 2006], *Lactobacillus brevis* [Angulo *et al.*, 2011], *Streptococcus thermophilus* [Angulo *et al.*, 2011], *Clostridium perfringens* [Si *et al.*, 2004], *Bacillus cereus* [Gilbert and Kramer, 1984], *Listeria* species [Gonzalez-Zorn *et al.*, 1999; Vazquez-Boland *et al.*, 2001], and *Saccharomyces cerevisiae* [Ella *et al.*, 1997]). Others may be added to the list, as SMase expression by gut microbes has not been systematically analyzed. Because bacteria do not make SM, the physiological function(s) of bacterial SMase may be to modulate mucosal cell SM/ceramide levels, but how this would affect host enterocyte function and mucosal defense is not known.

Our interest in how the conversion of SM to ceramide via SMase might affect the apical membrane of polarized enterocytes emerged from our studies on CT. CT enters intestinal cells from the apical surface by binding its sphingolipid receptor ganglioside GM1. Like SM, GM1 has an affinity for lipid raft nanodomains, and these two sphingolipids coassemble and function together in such specialized membrane structures. We found earlier that in intestinal epithelial monolayers, the conversion of apical membrane SM to ceramide by exogenously applied bacterial SMase decreased endocytosis and toxicity of CT (Saslowsky and Lencer, 2008). The effect was fully reversible, specific to toxin entry via the apical membrane, and was recapitulated by addition of exogenous long-chain ceramides. In this article, we explore mechanisms that might explain these effects. Because cortical actin is linked to and affects the structure, function, and endocytosis of SM-containing lipid microdomains, including those bearing CT-GM1 complexes (Villalba *et al.*, 2001; Pelkmans *et al.*, 2002; Badizadegan *et al.*, 2004), we began by testing for effects of SMase on the apical actin cytoskeleton.

RESULTS

Conversion of apical SM to ceramide induces reorganization of the apical cortical actin cytoskeleton in polarized intestinal epithelia

We found that apically applied SMase from *S. aureus* induces a striking reorganization of F-actin localized to the apical region of polarized human T84 intestinal monolayers (Figure 1). Untreated control T84 monolayers not treated with SMase and fixed and stained with fluorophore-labeled phalloidin displayed an apical mesh-like network of F-actin with intact perijunctional actin rings, as visualized in en face optical confocal sections acquired at the plane of tight junctions (TJs; Figure 1A, left). In contrast, monolayers treated apically with SMase (0.75 U/ml) displayed a dense clustering of F-actin centralized in the plane of the apical membrane that extended 2–5 µm into the cell interior (Figure 1, A, right, and B, arrowheads, and Supplemental Movie S1). Greater than 60% of cells were affected, and SMase from other bacterial and human sources fully reproduced this alteration (unpublished data). Boiling SMase before monolayer application abolished the phenotype, consistent with

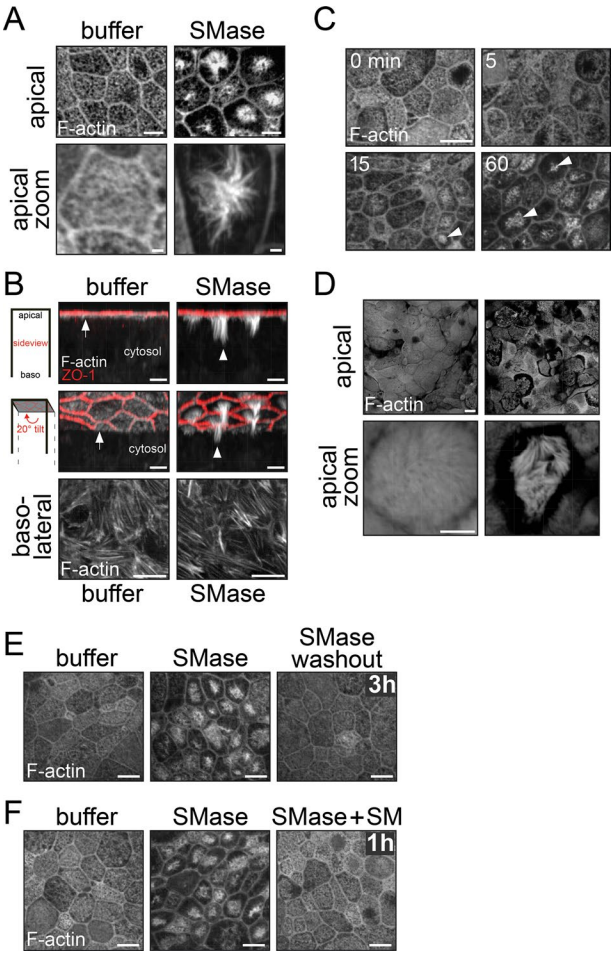

FIGURE 1: Apical conversion of SM to ceramide by SMase induces cortical F-actin reorganization in polarized intestinal epithelial monolayers. (A) T84 monolayers were incubated with or without bacterial SMase (1 U/ml) apically for 1 h, fixed, and F-actin stained with labeled phalloidin (imaged en face to monolayer). Bottom, digital magnifications showing single cells. (B) Images of T84 monolayers rendered from confocal Z-dimension stacks and displayed perpendicular to the plane of the monolayer (middle images are 20° rotations of top images). F-actin was detected as in A, and the TJ marker ZO-1 was detected by immunostaining. Arrow indicates cortical F-actin network underlying apical PM, and arrowhead indicates F-actin phenotype (also depicted in a rotatable movie format in Supplemental Movie S1). Bottom, single *XY*-planes showing basolateral stress fibers. (C) T84 monolayers incubated apically with SMase for the indicated times were fixed and imaged as in A. Arrowheads indicate cortical F-actin bundle structures. (D) Caco-2 monolayers incubated with or without SMase were fixed and imaged as in A. (E) Polarized T84 monolayers incubated apically for 1 h with buffer or 1 U/ml SMase were washed and incubated a further 3 h in buffer only (SMase washout) or (F) for 1 h in buffer containing 30 µM mixed long-chain SM species (SMase + SM). Bars, 10 µm (A–F), 1 µm (A, bottom), 5 µm (D, bottom).

the effect being dependent on enzymatic activity (unpublished data). SMase induced detectable changes in F-actin structure as early as 15 min after apical treatment, with the maximal effect occurring by 60 min (Figure 1C). SM depletion from the apical PM after SMase treatment was confirmed using a SM-binding probe (Supplemental Figure S1A; Saslowsky and Lencer, 2008). Monolayers of human Caco-2 intestinal cells treated apically with SMase also displayed altered F-actin morphology (Figure 1D), suggesting that the results can be generalized to other in vitro models of human intestinal epithelia. Of interest, SMase treatment had no detectable effect on cortical F-actin morphology in nonpolarized T84 or Caco-2 cells grown on glass coverslips (Supplemental Figure S1B and unpublished data), implicating a specific effect of SMase on the specialized actin assemblies forming the apical brush border of polarized epithelia.

The F-actin phenotype was completely reversible (Figure 1E), and apical repletion by addition of SM after SMase treatment decreased the recovery time to achieve normal F-actin morphology (Figure 1F). Remarkably, the perijunctional actin ring remained intact in all cells (Figure 1A, apical), and basolateral actin stress fibers were not detectably changed structurally (Figure 1B, bottom) or functionally (Saslowsky and Lencer, 2008). Pretreatment with the actin-stabilizing drug jasplakinolide abrogated the SMase-induced F-actin phenotype, suggesting that F-actin bundles are formed via de novo polymerization events and not by remodeling of existing structures (Supplemental Figure S1C). Apical SMase treatment had no obvious effect on the morphology of the TJ-associated protein ZO-1 (Figure 1B) or transepithelial resistance (TER; Saslowsky and Lencer, 2008), suggesting that TJs also remained intact. In addition, cAMP- and Ca^{2+}-dependent Cl^- secretion was not affected by apical SMase, showing that ion channel function at the apical PM remained generally intact and that ceramide formation was not compromising apical PM integrity (Saslowsky and Lencer, 2008; Saslowsky *et al.*, 2009).

To demonstrate that the SMase-induced phenotype can be elicited via host–microbe interactions, we performed coculture experiments with human T84 monolayers and *S. aureus* bacteria that synthesize and secrete a SMase enzyme (Hlb/β-hemolysin). T84 monolayers incubated apically for 75 min with wild-type, SMase-secreting *S. aureus* (multiplicity of infection [MOI] = 20; strain 8325-4) displayed a similar F-actin phenotype as when exposed to purified SMase alone (Figure 2, top left). Coculture of monolayers with an isogenic *S. aureus* strain harboring a viral-inactivating insertion in the β-hemolysin gene (MOI = 20; strain DU5719; Patel *et al.*, 1987) resulted in a completely normal actin cytoskeleton (Figure 2, bottom left), consistent with the F-actin phenotype being induced by SMase enzymatic activity. As with the purified enzyme, apical exposure of monolayers to *S. aureus* had no effect on basolateral stress fibers (Figure 2, right) or TER (unpublished data).

Our previous studies revealed a defect in CT uptake in intestinal epithelial cells treated apically with SMase, with ceramide generation being the decisive factor (Saslowsky and Lencer, 2008). The actin cytoskeleton has been implicated in CT uptake into endocytic pathway(s) leading to intoxication, suggesting that SMase-induced alterations in apical F-actin might explain the protective effect against CT. To test this idea, we used a pathogenic microbe that requires actin for invasion: *Salmonella typhimurium*. Apical preincubation of T84 monolayers with SMase resulted in ~50% less invasion through the apical membrane by wild-type *S. typhimurium* compared with controls (Figure 3, left and middle columns). Assay background was determined using the *S. typhimurium* isogenic mutant VV341, which features a deletion of the *hilA* locus, rendering it incapable of invading cells (Bajaj *et al.*, 1995; Hueck *et al.*, 1995; Figure 3, right column). The magnitude of the block in *Salmonella* invasion was similar to that observed for inhibition of CT toxicity (Saslowsky and Lencer, 2008). Because only a fraction (~60%) of SMase-treated cells display the F-actin phenotype, we consider it likely that such cells are highly or even completely resistant to invasion.

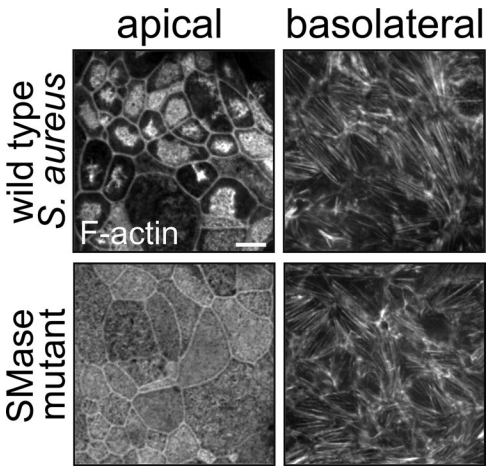

FIGURE 2: SMase secretion by live bacteria induces cortical F-actin reorganization. T84 monolayers were incubated apically with wild-type *S. aureus* or a mutant devoid of SMase activity (MOI = 20) for 1 h, fixed, and F-actin imaged as in Figure 1. Bar, 10 μm.

The SMase-induced F-actin phenotype could be caused by the generation and accumulation of membrane ceramide, loss of SM, perturbation of cholesterol homeostasis, or release and downstream action of the phosphorylcholine SM head group. The last-named possibility was rejected because monolayers incubated apically with a range of phosphorylcholine concentrations showed no change in apical F-actin morphology (unpublished data). Similarly, depletion of cholesterol from the apical PM by extraction with methyl-β-cyclodextrin (MβCD) did not obviously change corticular F-actin structure (Supplemental Figure S1, D and E), suggesting that alterations in membrane cholesterol content, on their own, cannot explain

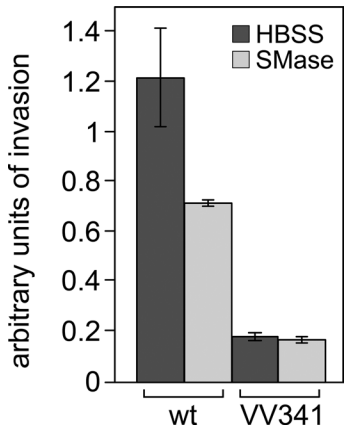

FIGURE 3: Apical SMase treatment attenuates *S. typhimurium* invasion. Polarized T84 monolayers were treated apically with 1 U/ml SMase for 1 h apically before apical *S. typhimurium* incubation. After gentamicin treatment at 4°C for 1 h and extensive washing, only intracellular bacteria are viable. VV341 harbors a mutation rendering it incompetent to invade cells. $n = 3$ for each condition.

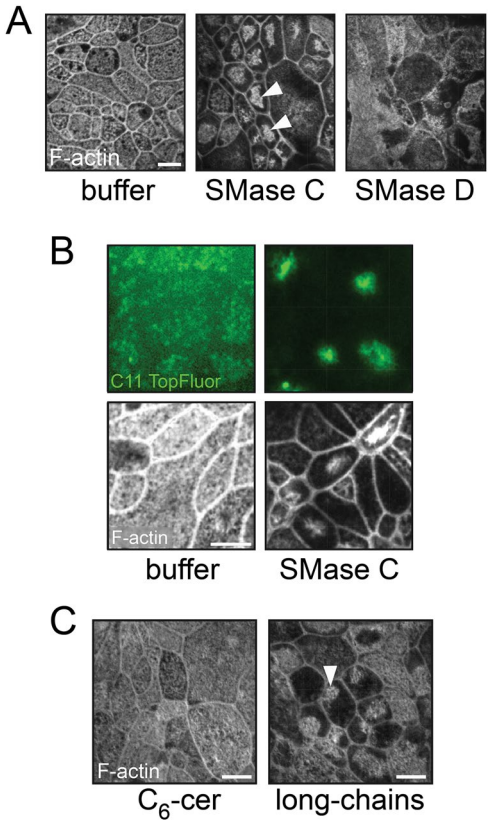

FIGURE 4: Apical ceramide is necessary and sufficient to induce changes in cortical F-actin structure. (A) T84 monolayers treated apically with 1 U/ml indicated SMase were fixed and imaged as in Figure 1. (B) As in A, except that the fluorescent ceramide C11 TopFluor ceramide was incubated for 15 min after SMase C/buffer treatment and imaged in live cells by confocal microscopy. (C) T84 monolayers were incubated for 2 h apically with either short-chain (C6) or mixed long-chain ceramides complexed with α-cyclodextran, fixed, and imaged as in A. Bars, 10 μm.

the SMase-induced phenotype. To determine whether the loss of SM or accumulation of ceramide was the decisive factor, we incubated monolayers with SMase D from *Corynebacterium pseudotuberculosis*. This enzyme cleaves SM at a different position, one phosphate group higher, leaving ceramide-1-phosphate (C1P) in the outer PM leaflet instead of ceramide (Subbaiah *et al.*, 2003). Apical SMase D treatment depleted the apical membrane of SM (Supplemental Figure S1F) but failed to elicit the same phenotype as *S. aureus* SMase (also known as SMase C; Figure 4A), although it did cause a loss of perijunctional actin staining and a more-diffuse-appearing cortical actin network (Figure 1F, right). SMase D treatment also abolished TER (unpublished data), unlike what we observe with SMase C from *S. aureus*. This shows that SM loss from the apical PM cannot explain our results.

To test whether the PM region overlying the SMase-induced F-actin structures was enriched in ceramide, we incorporated the fluorescent ceramide tracer C11 TopFluor ceramide into the apical membranes of SMase-treated or untreated T84 cells. The results show that in live cells, C11 TopFluor ceramide is distributed across the apical surface of control (untreated) monolayers, with small areas of enrichment evident in the focal plane of the apical PM of individual cells (Figure 4B, top left). In contrast, SMase pretreatment of T84 monolayers caused the fluorescent ceramide tracer to concentrate in dense foci of the apical membrane (Figure 4B, top right), spatially consistent with the condensed F-actin structures induced by SMase (Figure 4B, bottom). We also found that addition of exogenous long-chain but not short-chain (C6) ceramides partially recapitulated the cortical actin phenotype (Figure 4C). Thus it is the generation of long-chain ceramide in the apical membrane that explains the F-actin phenotype, consistent with our previous findings with respect to CT toxicity (Saslowsky and Lencer, 2008). Although the de novo apical membrane ceramide generated by the SMase C reaction might flip to the inner PM leaflet and undergo conversion to C1P and other metabolites, this cannot explain our results, as pretreatment of monolayers with the ceramide kinase inhibitor NVP-231 failed to block the F-actin phenotype (unpublished data). In addition, we found no evidence for ceramide (via SMase treatment or exogenously added long-chain species) inducing apoptosis in T84 monolayer as assayed by annexin V staining of the outer PM leaflet (unpublished data). The results are consistent with the formation of large, ceramide-rich apical membrane domains.

The striking change in cortical F-actin structure prompted us to examine whether other subcellular features of the BBM or intracellular organelles might be affected by conversion of apical SM to ceramide. Transmission electron microscopy showed microvillar effacement in the central region of cells overlying the region of F-actin rearrangement in T84 monolayers (Figure 5A). By confocal microscopy, we found that microtubules extended deeper into the cell interior and essentially encased the SMase-induced F-actin bundles without obviously penetrating those structures (Figure 5B). Immunolocalization of the endoplasmic reticulum (ER)–resident protein calnexin showed an obvious relocalization of calnexin away from the central, subapical region of each cell in monolayers treated apically with SMase as compared with buffer controls (Figure 5C). This is the approximate area of the F-actin bundles, which, we infer, physically excluded the ER from these sites. We did not observe any changes in the intracellular distribution or morphology of the Golgi or recycling endosomes, as visualized by GM130 or Rab11 immunostaining (Figure 5, D and E, respectively), nuclei, or the early or late endosomal compartments (gauged by EEA1 and LAMP1 immunostaining, respectively; unpublished data), consistent with their more basal and perinuclear localizations within polarized epithelial cells.

GM1, cholesterol, and phosphatidylinositol (4,5)-bisphosphate are depleted from the PM overlying SMase-induced F-actin structures

Our tracer studies suggest that the ceramide produced during SMase exposure self-assembles into large, micrometer-sized domains. Such ceramide rich domains are known to exclude certain lipid raft components, including SM and cholesterol (Megha and London, 2004; Taniguchi *et al.*, 2006; Sot *et al.*, 2008). To test whether this occurs in our model system, we used fluorescently labeled cholera toxin B-subunit (CTB), which binds the lipid raft marker ganglioside GM1 with high specificity and affinity. In buffer-treated monolayers, fluorophore-labeled CTB was distributed across the full apical surface of individual cells, and F-actin displayed a uniform, mesh-like network underlying the apical PM (Figure 6A, top). In SMase-treated monolayers, however, CTB localized GM1 to regions of the apical membrane almost exclusively outside of the regions overlying the centralized, F-actin bundles (Figure 6A, bottom, outlined in red). The segregation of CT-GM1 complexes from the dense F-actin core in SMase-treated cells was also observed in monolayers labeled with native CTB and assessed by immunofluorescence using antibodies against CTB (unpublished data). Thus

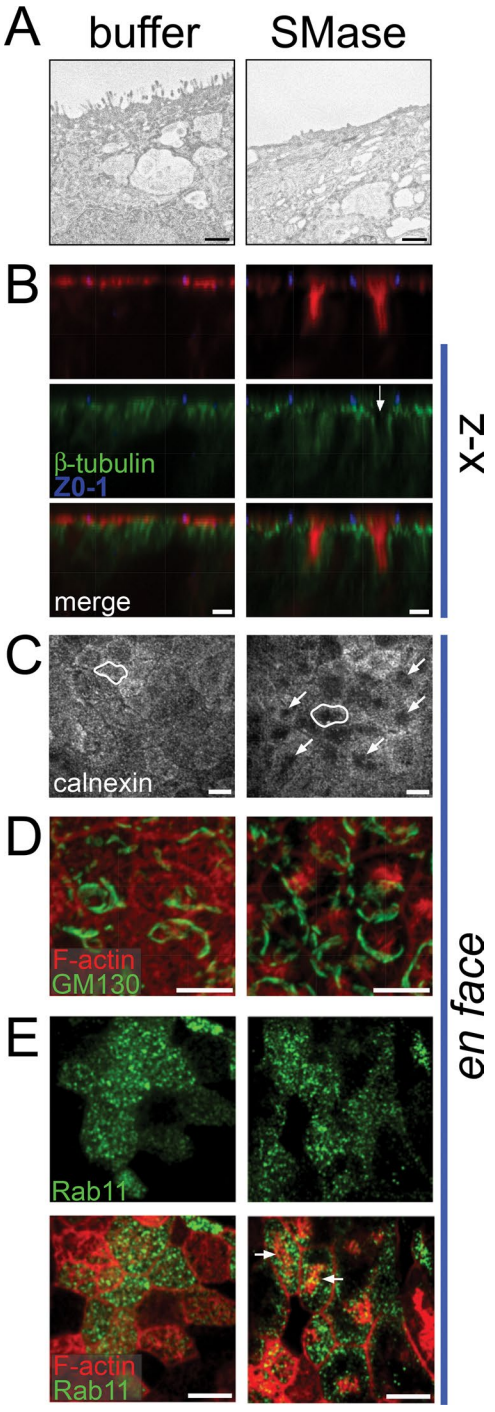

FIGURE 5: Effects of SMase on polarized T84 subcellular structure. (A) Transmission electron microscope micrographs of T84 monolayers incubated apically with or without SMase for 50 min. Ultrathin sections are perpendicular to the monolayer support. Scale bar, 1 μm. Box insets are 2× digital zooms of apical PM region. (B) Three-dimensional reconstructions from *XY*-stacks of monolayers stained with phalloidin and immunostained for ZO-1 and β-tubulin. Arrow denotes lack of microtubules in the internal region of the SMase-induced F-actin bundle structure. (C) Monolayers treated with or without SMase were methanol fixed and immunostained for the ER marker calnexin (a fixation method not compatible with phalloidin staining). Enclosed areas represent single-cell outlines, and arrows denote regions of decreased calnexin immunostaining in SMase-treated monolayers. (D) Monolayers treated with or without SMase were fixed and immunostained for the Golgi marker GM130 or (E) Rab11 to mark recycling endosomes (arrows denote region of altered F-actin structure for the latter). Scale bars, 1 μm (A), 10 μm (B–E).

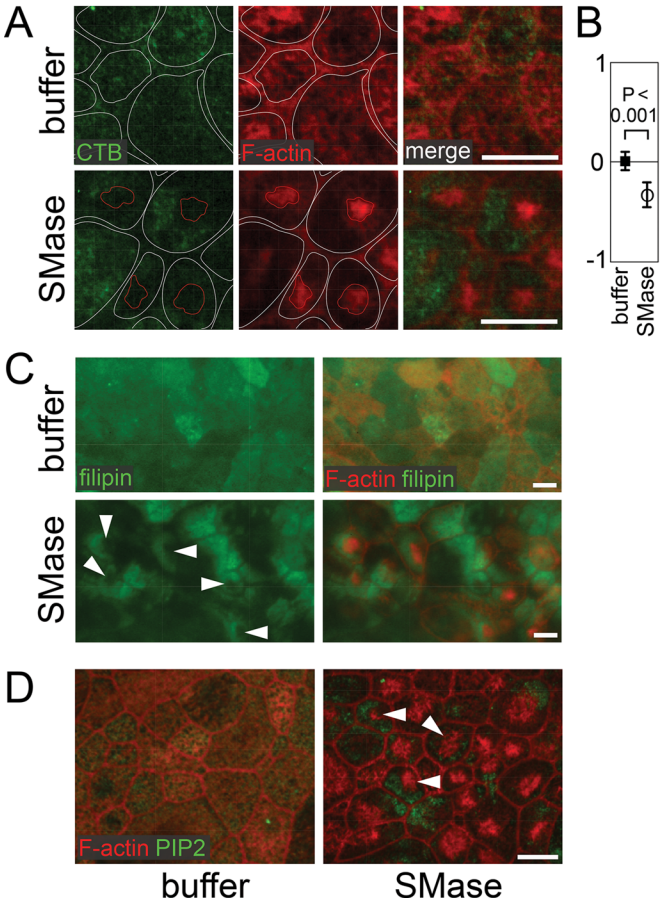

FIGURE 6: CTB, cholesterol, and PIP2 are depleted from the central PM region overlying SMase-induced F-actin structures. (A) T84 monolayers were incubated apically with or without SMase at 37°C, incubated with 10 nM fluorophore-labeled CTB at 4°C, fixed, stained for F-actin, and imaged by confocal microscopy at the plane of the apical PM. The hand-drawn white lines approximate individual cells exclusive of the perijunctional F-actin ring, and the red lines approximate the SMase-induced F-actin bundle structures. (B) Correlation analysis of CTB and F-actin fluorescence signal in T84 monolayers treated with or without SMase ($p < 0.001$). (C) As in A, except that cholesterol was stained with filipin or (D) PIP2 was immunostained using anti-PIP2 immunoglobulin M. Arrowheads in C and D denote PM domains overlying the F-actin bundle structures. Scale bars, 10 μm.

conversion of SM to ceramide causes a redistribution of F-actin to the central region of the apical membrane, and this coincides with the redistribution of the CTB-GM1 complex away from the PM region overlying the F-actin bundles to peripheral regions of the apical PM outer leaflet.

To quantify the redistribution, we calculated the Pearson's correlation coefficient (ρ) for colocalization of CTB and cortical F-actin. Image analysis of 90 individual cells from untreated monolayers showed that the fluorescence signals representing CTB and F-actin possess virtually no correlation (ρ = 0.012 ± 0.075 SD;

Figure 6B), meaning that the two species have a random distribution of fluorescence intensities with respect to each other across the plane of the apical PM. In contrast, the analysis of the same number of cells from SMase-treated monolayers showed a negative correlation for the fluorescence intensities between CTB and F-actin ($\rho = -0.328 \pm 0.098$ SD). In other words, in SMase-treated monolayers, regions of the PM with higher intensities of fluorescence from CTB tend to have significantly ($p < 0.001$) less fluorescence from F-actin (Figure 6B). A similar redistribution of cholesterol and phosphatidylinositol (4,5)-bisphosphate (PIP2) away from cortical F-actin was observed in the apical PM of SMase-treated cells, as assessed by the location of the sterol-binding molecule filipin and PIP2 immunolocalization (Figure 6, C and D, respectively). Thus, converting SM to ceramide caused canonical lipid raft–associated lipids resident in both inner and outer leaflets of the apical PM to redistribute away from the region overlying cortical F-actin bundle structures.

The ezrin/radixin/moesin (ERM) family of actin-regulating proteins plays an important role in cortical F-actin and brush border membrane dynamics in polarized epithelia (Bretscher, 1999; Saotome *et al.*, 2004). Because the ERM proteins are coregulated by membrane PIP2 (Bretscher *et al.*, 2002), we tested whether they also might be involved in the SMase-induced phenotype by localizing them in relation to the SMase-induced actin bundles. Immunolocalization studies in untreated T84 monolayers showed that ezrin and ezrin-binding protein 50 (EBP50) distributed with cortical F-actin across the apical PM, but they were excluded from TJ regions (Figure 7, A and B, top). In SMase-treated monolayers, however, the location of both ERM proteins was altered. Each colocalized with the F-actin bundles induced by SMase (Figure 7, A and B, bottom). In contrast to the ERM proteins, immunofluorescence of Myosin 1a showed no change in the lateral distribution of Myo1a across the apical PM, indicating that only certain cortical F-actin and microvillar effectors are affected by SMase treatment (Figure 7C).

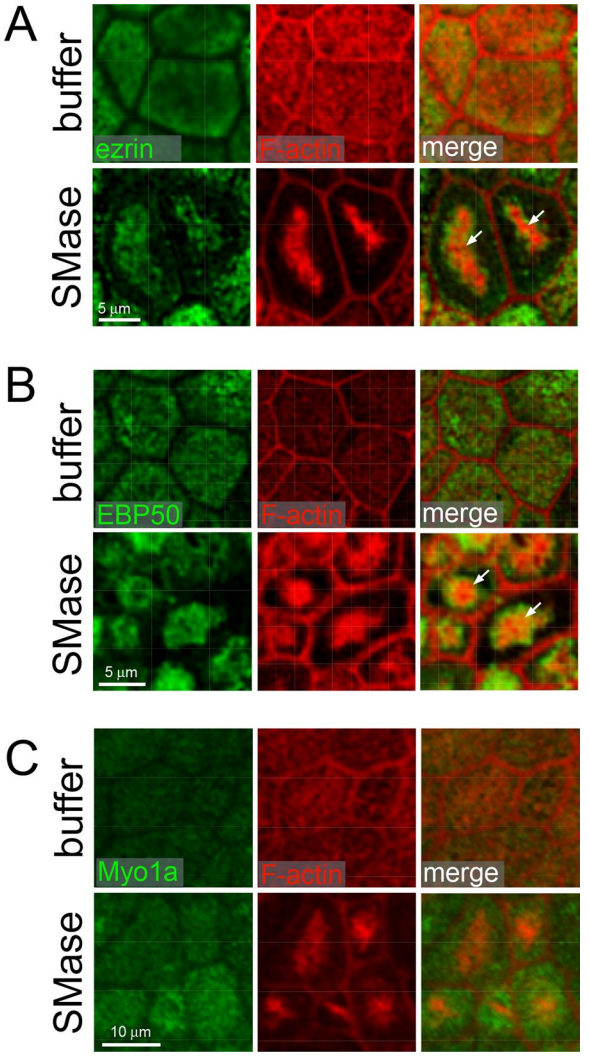

FIGURE 7: Ezrin and EBP50 coalesce with SMase-induced cortical F-actin structures. T84 monolayers incubated apically with or without SMase were fixed and immunostained for ezrin (A), EBP50 (B), or myosin 1a (C), and F-actin was stained with labeled phalloidin in all cases. Arrows denote colocalization of ezrin and EBP50 with SMase-induced F-actin bundle structures. Scale bars, 5 µm (A, B), 10 µm (C).

RhoA activation by SMase action

The Rho-family GTPases Rac, Rho, and Cdc42 can act as F-actin effectors, are upstream mediators of ERM protein function (Bretscher *et al.*, 2002), and can be regulated by PIP2 (Hilpela *et al.*, 2004). A previous study showed that pharmacological inhibition of Rho-associated coiled-coil protein kinase (ROCK), a downstream Rho effector, resulted in a cortical F-actin phenotype in T84 monolayers similar to SMase treatment (Walsh *et al.*, 2001), although this does not exactly phenocopy SMase-induced actin changes, as the small molecule Y27632 used in that study also compromises the perijunctional actin ring (Supplemental Figure S2). Thus, to test whether activation of Rho family GTPases was involved, we affinity isolated the active (GTP-bound) forms of RhoA, Cdc42, and Rac1 in SMase-treated and control T84 monolayers. Whereas the activation state of Cdc42 and Rac1 was not affected (unpublished data), apically applied SMase induced a transient 3.4-fold increase in RhoA activation (±0.3-fold), which preceded the structural changes in F-actin (Figure 8A, compare lanes 3 and 4). This initial burst of RhoA activity rapidly diminished to below control levels (Figure 8A, lane 5; 0.9-fold compared with lane 3).

To test whether RhoA activation was required for the SMase-induced phenotype, we first attempted to genetically deplete RhoA, but this resulted in T84 cells incapable of forming functional monolayers and precluded an experiment (unpublished data, supported by Nusrat *et al.*, 1995). Therefore we instead used the RhoA-inactivating toxin from *Clostridium difficile* (TcdA; Just *et al.*, 1995). Pretreatment of T84 monolayers with TcdA before SMase incubation should block the induction of F-actin bundle structures if RhoA activation is required. Preliminary studies showed that TcdA concentrations >0.5 nM could not be used because, on their own, they induced aberrant, cell-wide alterations in F-actin morphology and loss of TJ function (Supplemental Figure S3; Riegler *et al.*, 1997; Feltis *et al.*, 2000). Submaximal doses of TcdA toxin, however, did not induce obvious, deleterious alterations in F-actin structure, although we presume that some fraction of total RhoA was still affected at such lower doses of TcdA. As shown in Figure 8, monolayers incubated with low-dose, 0.2 nM TcdA displayed only minor structural changes in cortical F-actin structure (compare Figure 8, B and C), and they were refractory to SMase-induced cortical F-actin reorganization (Figure 8, compare D and F with E and G). The effect was quantified by scoring individual cells within the monolayer as having either a normal or SMase-phenotypic apical cortical F-actin structure (as defined in Figure 1). In buffer-treated monolayers, >90% of the cells displayed a normal F-actin morphology regardless of pretreatment with either buffer or 0.2 nM TcdA (Figure 8H, first two bars). In

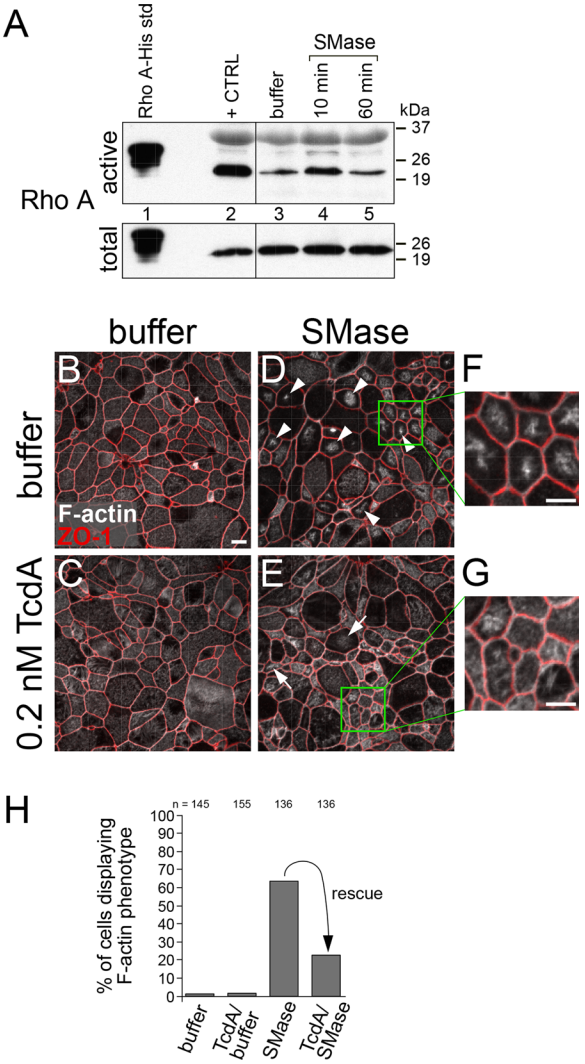

FIGURE 8: RhoA activation is required for the cortical F-actin phenotype induced by apical SMase treatment. (A) GTP-bound Rho (active form) was affinity isolated from T84 monolayer protein lysates and analyzed for RhoA by immunoblot (top). Bottom, RhoA immunoblot of input protein lysates to demonstrate RhoA equivalence among sample extracts. A 20-ng amount of purified histidine-tagged RhoA was loaded as standard (lane 1). Experimental samples (lanes 3–5) were treated with buffer only (60 min) or 1 U/ml SMase for the indicated times. Positive controls (lane 2) were produced by incubating lysates from parallel samples with an excess of GTPγS to preload RhoA, locking it in an "active" state. Molecular weight standards are indicated at the left. (B–G) T84 monolayers were preincubated with buffer or TcdA for 1 h before the addition of buffer or 0.5 U/ml SMase for an additional 1 h. F-actin and ZO-1 were imaged as in Figure 1B, but en face to monolayer. Arrowheads indicate SMase-induced F-actin bundles, and arrows denote attenuated bundle formation in TcdA-pretreated monolayers. (F, G) Digital zooms of the boxed areas in D and E, respectively. Scale bars, 10 μm. (H) Quantitation of results depicted in Figure 6, B–G. Based on F-actin morphology, cells populating fields of view in confocal optical sections from three independent experiments were scored for displaying the F-actin phenotype (bundling and concentration in the central region underlying the apical PM). Total number of cells analyzed/condition is indicated above the bars. Data are representative of at least three independent experiments.

SMase-treated monolayers, TcdA pre-treatment rescued the normal actin-phenotype by approximately threefold (Figure 8H, last two bars). These results suggest that RhoA activation is required for induction of the observed F-actin bundles and implicate microbial SMase-induced ceramide microdomains as regulators of RhoA signaling at the apical BBM of the human intestine.

DISCUSSION

The results of this study show that enzymatic conversion of SM to ceramide in the apical membrane of polarized intestinal cells causes large-scale domain formation and restructuring of the apical, cortical F-actin network underlying the PM. It appears that after liberation from SM, ceramide forms its own macrodomain, which excludes cholesterol and CT–GM1 complexes, ablates microvilli, and somehow nucleates the dramatic F-actin rearrangement. The bulk of ceramide overlying the SMase-induced F-actin bundles are likely long-chain ceramides. This ceramide-induced actin phenotype can be induced by a microbial species common to the gut microflora and is dependent on RhoA activation. The combined effects of membrane lipid domain alterations and F-actin restructuring result in resistance to invasion by the gut pathogen *Salmonella* and cholera toxin and perhaps by other microbes and microbial products that coopt the apical actin cytoskeleton to enter host cells.

Reorganization of the apical cortical actin cytoskeleton

A striking finding from this study is the effect of SMase action on apical, corticular F-actin structure and how CT–GM1 complexes and cholesterol on the outer leaflet of the apical PM segregate away from the overlying PM region. The SMase/ceramide-induced reorganization of the apical F-actin cytoskeleton is distinct from other reports of F-actin reorganization in polarized cells (Hecht *et al.*, 1988; Madara *et al.*, 1988; Ivanov *et al.*, 2004). Only the F-actin underlying the apical PM is affected, and there are no effects on TJs, as assessed functionally by TER and morphologically by immunostaining for ZO-1. SMase does not affect perijunctional actin rings or basolateral stress fibers, and neither protein kinase C (PKC) nor phospholipase C, enzymes involved in F-actin remodeling, mediate the SMase-induced reorganization in apical F-actin. Such selective disruption of cortical F-actin without impairment of TJ structure/function is a unique finding and may be an important way that luminal gut microbes affect the BBM to limit uptake and lysosomal degradation. Because the PM regions overlying the condensed F-actin structure exclude the CTB-subunit bound to GM1 in polarized intestinal epithelial cells, we propose that our previous findings (that SMase inhibits toxicity and CT-GM1 endocytosis) are explained by alterations in corticular F-actin structure and function.

The ability of SMase to induce the observed phenotypes at the apical PM is likely to be specific for SM species containing long acyl chains because only exogenous long-chain ceramides recapitulate the SMase-induced alterations in F-actin bundle formation. These findings correlate well with our previous studies showing that apically loaded long- but not short-chain ceramides inhibit cholera intoxication from the apical PM (Saslowsky and Lencer, 2008). Note that the C1P generated by SMase D action cannot flip between bilayers as readily as ceramide, and this may be important for how ceramide acts to deform the membrane. Although ceramide can be converted into the potent signaling molecule S1P (Merrill *et al.*, 1997), this does not explain our results, as exogenous S1P addition had no effect on F-actin structure or CT toxicity, and we never observed activation of extracellular signal–regulated kinase signaling as would be expected if S1P was generated at significant levels

(Saslowsky and Lencer, 2008; Saslowsky *et al.*, 2009; unpublished data). In T84 cells, cholesterol depletion does not microscopically change apical cortical F-actin structure, although CT endocytosis and toxicity are inhibited by cholesterol depletion using cyclodextrins (Wolf *et al.*, 2002). Because ceramide has a strong tendency to self-assemble into large microdomains and exclude cholesterol (Grassme *et al.*, 2003; Gulbins *et al.*, 2004), it is possible that ceramide acts indirectly to affect CT function by perturbing PM cholesterol dynamics. This possibility is supported by our finding that cholesterol is depleted in the central PM domain overlying the ceramide-induced F-actin bundles.

Our results showing a redistribution of the ERM proteins ezrin and EBP50 to the F-actin bundles imply that apical conversion of SM to ceramide disrupts the normal tethering of cortical F-actin to the apical PM without compromising the ability of F-actin to interact with these effector proteins. We presume that this is due to nascent ceramide domains forming in the outer apical PM leaflet and disrupting the normal ERM–PM associations. The mechanism underlying this redistribution, however, is unexplained. In nonpolarized MCF-7 cells (Zeidan *et al.*, 2008), exogenous SMase induces dephosphorylation of ezrin via the action of PKCδ, but this does not explain our results, as inhibition of PKCδ by calphostin C failed to block SMase-induced F-actin and ezrin reorganization (unpublished data).

SMase-induced alterations in apical membrane microdomains

How the conversion of SM to ceramide in the outer leaflet of the PM actuates the reorganization of F-actin microfilaments is not known. One possibility is that the enzymatic action of SMase displaces a cortical actin anchor protein(s) or lipid (such as PIP2) from membrane nanodomains, thus compromising the ability of F-actin to fully and uniformly distribute across the inner leaflet of the apical cell PM. We suspect that PIP2 is a key player in the apical SMase phenotype because it normally partitions into the inner-leaflet, sphingomyelin-containing lipid raft nanodomains (Liu *et al.*, 1998; Pike and Miller, 1998) but becomes excluded from the central, presumably ceramide-rich domain induced by SMase treatment (Figure 6D). PIP2 regulates actin dynamics by binding and modulating the activity of actin effectors, including N-WASP (Ho *et al.*, 2004), small GTPases such as Rac, Rho, and Cdc42 (Hilpela *et al.*, 2004), and members of the ERM family (Bretscher *et al.*, 2002). Our findings that apical SMase transiently activates RhoA and concomitantly causes redistribution of ezrin, PIP2, and EBP50 raises the possibility that disruption of apical microdomains may mediate the process. One possibility would be that ceramides produced by SMase disrupt the PIP2-containing inner leaflet microdomains either by flipping to the inner leaflet and coalescing or through transbilayer effects via long, saturated acyl-chain interactions (Devaux and Morris, 2004; Gri *et al.*, 2004). These ideas are supported by a study by Abe *et al.* (2012), who found that during cytokinesis (in HeLa cells), SM and PIP2 are concentrated in the outer and inner leaflets, respectively, of the membrane bilayer comprising the cleavage furrow. After exogenous SMase treatment, they no longer detected PIP2 concentration at this site, RhoA accumulated to a lesser extent, and cytokinesis was impaired. Of interest, cholesterol was also enriched at the cleavage furrow, a feature not affected by SMase action, analogous to what we find in the present studies. Whether any of the phosphatidylinositides or ERM proteins plays a direct role in alteration of brush border structure remains to be determined.

In vivo relevance

The activities of the exogenous SMases on apical brush border membranes might have clinical relevance. Of the 100 trillion commensal microbes colonizing the gut, some produce SMase, as do certain microbial pathogens (Gonzalez-Zorn *et al.*, 1999; Angulo *et al.*, 2011). This, we predict, will alter the brush border of intestinal cells in ways described here, although perhaps without the dramatic progression to microvillar loss and large-scale cortical F-actin rearrangement seen in vitro. Still, such transient SMase-induced disruption of lipid rafts by formation of ceramide microdomains and Rho-dependent alterations in actin structure and function are predicted to have physiological consequences. This is perhaps best evidenced by the resistance we observe against cholera toxin (Saslowsky and Lencer, 2008) and Salmonella invasion (this study). It is also possible that in some instances, disruption of lipid nanodomains by depletion of SM on its own, separate from the induced F-actin rearrangements, may account for resistance to infection against some microbes and viruses. Recent studies, for example, show that by binding to the glycosphingolipid GB3, *P. aeruginosa* can induce the early stages of cell invasion by "zippering" lipid rafts around the organism as it induces inwardly directed membrane curvature (Eierhoff *et al.*, 2014). The invaginations depend on lipid raft structure but not on actin dynamics. In the case of *Pseudomonas aeruginosa*, actin dynamics is still required for microbial invasion and pathogenesis, but this may not be true for other microbes or viruses. Overall, our results implicate the microbial SMases as one way in which gut microbes might modulate the epithelial barrier so as to affect innate host defense and enhance or disrupt intestinal homeostasis.

MATERIALS AND METHODS

Reagents

Long-chain porcine brain ceramides or sphingomyelins and synthetic C6 ceramide were from Avanti Polar Lipids (Alabaster, AL), bacterial SMase (*S. aureus*) was from Sigma-Aldrich (St. Louis, MO), goat anti-calnexin was from Santa Cruz Biotechnology (Dallas, TX), anti–phospho-ezrin was from Cell Signaling Technology (Danvers, MA), anti-PI(3,4)P2 was from Eschelon Biosciences (Salt Lake City, UT), anti-GM130 was from Abcam (Cambridge, MA), CTB–Alexa Fluor 488 conjugate, phalloidin–Alexa Fluor 568, and mouse anti-ZO1 were from Thermo Fisher Scientific (Waltham, MA), anti-CTB was used as previously described (Saslowsky *et al.*, 2013), and C11 TopFluor ceramide was from Avanti Polar Lipids. Hanks' balanced salt solution (HBSS), pH 7.4, was used for all manipulations with live cells. Recombinant lysenin fused to red fluorescent protein was a kind gift from Toshihide Kobayashi (RIKEN, Japan). This fusion protein contains a truncated form of lysenin that cannot oligomerize but still binds SM specifically (Kiyokawa *et al.*, 2005). Other kind reagent gifts were as follows: *C. difficile* TcdA was from Borden Lacy (Vanderbilt University); SMase D from *C. pseudotuberculosis* was from Yvonne Lange (Rush University Medical Center) and Yusuf Hannun (Stony Brook University); anti-EBP50 and anti-ezrin were from Anthony Bretscher (Cornell University); anti-Myo1a was from Mark Mooseker (Yale University); and rabbit anti-Rab11 was from Jim Goldenring (Vanderbilt University). All other chemicals and reagents were from Sigma-Aldrich.

Cell culture

Polarized monolayers of human T84 cells were cultured on 0.33- (for imaging) or 5-cm^2 (for biochemistry) polyester Transwell inserts (Corning, Acton, MA) as previously described (Lencer *et al.*, 1995).

S. aureus growth conditions

Bacterial cultures were grown overnight with aeration at 37°C in tryptic soy broth. The bacteria were pelleted, washed once in 0.01 M phosphate and 0.15 M NaCl, pH 7.2, and resuspended in the same buffer.

RhoA activation assay and immunoblot analysis

T84 monolayers grown on 5-cm^2 inserts were assayed for RhoA activation using a commercially available assay kit (Cytoskeleton, Denver, CO). Lysates from two inserts were pooled for each sample, and 800 µg of crude lysate was used to produce the positive control. SDS–PAGE (10–20% Tris-HCl gradient gels) and standard immunoblotting methodologies were as previously described (Saslowsky and Lencer, 2008), using manufacturer-supplied anti-RhoA antibody. Band intensity was quantified by densitometric analysis using ImageJ software (National Institutes of Health, Bethesda, MD). The relative intensities of the active RhoA bands were normalized to image background as well as total RhoA control bands.

Confocal microscopy

Lysenin fused to red fluorescent protein (2 mg/ml) was applied apically for either 60 min at 4°C or 5 min at 37°C to untreated and SMase C– or D–treated (1 U/ml, 50 min, 37°C) T84 monolayers. Monolayers were then washed, fixed with 4% paraformaldehyde (PFA) for 20 min, and mounted on slides using ProLong Gold Antifade reagent (Thermo Fisher Scientific). For immunolocalization studies, polarized T84 monolayers were treated and fixed as described and permeabilized using 0.2% saponin for 30 min at room temperature. Cells were washed, blocked in 10% nonimmune goat serum, and immunostained using the indicated primary antibody and then incubated with Alexa Fluor–conjugated secondary antibodies (Thermo Fisher Scientific) with or without the inclusion of Alexa Fluor–conjugated phalloidin to detect F-actin. For C11 TopFluor ceramide studies, polarized T84 monolayers (0.33-cm^2 inserts) were treated apically for 1 h with SMase (1 U/ml) or HBSS, washed, and then incubated with 2.5 µM C11 TopFluor ceramide for 15 min. Inserts were mounted in a microperfusion chamber and imaged as indicated later. Parallel inserts were fixed (4% PFA) and stained with Alexa Fluor 568–labeled phalloidin.

All samples were imaged by confocal microscopy on a Zeiss inverted Axiovert 200M microscope (Zeiss, Peabody, MA) coupled to a PerkinElmer-Cetus CSU-X1 spinning-disk confocal unit (Boston, MA), using a Zeiss 63× (1.4 numerical aperture) oil immersion objective lens and a QuantEM 512SC electron-multiplying charge-coupled device camera (Photometrics, Tucson, AZ). SlideBook software (Intelligent Imaging Innovations, Denver, CO) was used for image capture and processing. For rendering *XZ*-planes, stacks of *XY*-images were acquired at 0.3-µm intervals.

Colocalization analysis

Regions similar to the ones delineated with white lines in Figure 6A were analyzed for pixel correlation of the two channels for 90 cells each in images of SMase-treated and untreated (buffer) monolayers. This measurement was taken from optical sections that included both leaflets of the apical PM but excluded the apical perijunctional actin ring, which is not affected by SMase treatment. By definition, only cells that responded to SMase by aggregation of the cortical actin cytoskeleton were analyzed for the SMase set (representing ~60% of cell population). That ~60% of cells display the F-actin phenotype after SMase treatment is likely due, in large part, to T84 cells being a morphologically and functionally heterogeneous cell line. Strikingly, ~10–20% of cells in typical monolayers have much larger than average (~4–10×) apical diameter and lack any evidence of apical cortical F-actin (presumably no apical microvilli), and we have always considered these cells to be undifferentiated. As for visual scoring of the alteration in F-actin structure, only cells showing clear F-actin changes were counted (e.g., cells denoted by arrows in Figure 1C). Thus the remaining 20–30% of cells may have shown subtle changes in F-actin after SMase treatment but were not counted as positive for the phenotype (some cell examples of this are evident in Figure 1C, no arrows).

The *Y*-axis in Figure 6B is the Pearson's correlation coefficient, where +1 indicates perfect positive correlation of CTB and F-actin signal distribution, 0 indicates no correlation (random distribution), and −1 indicates perfect negative correlation (mutually exclusive distribution).

Electron microscopy

T84 monolayers grown on 0.33-cm^2 Transwell inserts were fixed, embedded, processed, and imaged as previously described (Madara *et al.*, 1987; Nusrat *et al.*, 1992) using a JEOL 1200EX electron microscope (Peabody, MA).

S. typhimurium invasion assay

Polarized T84 monolayers (0.33-cm^2 inserts) were treated apically with 1 U/ml SMase for 1 h at 37°C and washed three times, and then *S. typhimurium* (wild-type strain SL1344 or the isogenic mutant VV341) was added to the apical chamber for 1 h at 37°C. After washing, gentamicin was added as previously described (Criss *et al.*, 2001). After gentamicin treatment at 4°C for 1 h and extensive washing, only intracellular bacteria remain viable.

Lipid incorporation into cell membranes

Lipids or solvent (100% ethanol) were titrated into buffer containing 0.034% defatted bovine serum albumin to a final concentration of 30 µM as previously described (Pagano *et al.*, 1991). For incorporation of C6 and mixed long-chain ceramides into apical membranes, these species were titrated to a final concentration of 10 µM into 8 mM α-cyclodextrin in HBSS at 50°C to form a water-soluble complex and were applied apically to monolayers for 2 h. For cholesterol depletion, monolayers were incubated in 3 mM MβCD apically for 50 min. To quantify cholesterol depletion after the 50 min incubation, a fraction of the apical Transwell chamber contents was collected and assayed using an Amplex Red cholesterol assay kit (Thermo Fisher Scientific) per manufacturer's protocol. Briefly, pure 3 mM MβCD in HBSS was used as a blank in the assay, and experimental samples were directly compared with cholesterol standard curves (both with and without the inclusion of MβCD, which did not influence the assay results).

ACKNOWLEDGMENTS

We thank Marian Neutra for discussions and critical reading of the manuscript, Wendy Kam, Lydia Kaoutzani, and Meredith O'Hear for help with tissue culture, Jessica Wagner with image analysis, and Dan Chinnapen and Elisha Fielding for assistance with recombinant protein expression and purification. This work was supported by National Institutes of Health Grants R01 DK048106 to W.I.L., DK056754 and DK033506 to B.A.M., and K01 DK073480 and RO3 DK084090 to D.E.S., Pediatric Scientist Development Program K12-HD000850 to J.R.T., P30 DK034854 to the Harvard Digestive Diseases Center, and a Boston Children's Hospital Career Development Award to D.E.S.

REFERENCES

Abe M, Makino A, Hullin-Matsuda F, Kamijo K, Ohno-Iwashita Y, Hanada K, Mizuno H, Miyawaki A, Kobayashi T (2012). A role for sphingomyelin-rich lipid domains in the accumulation of phosphatidylinositol-4,5-bisphosphate to the cleavage furrow during cytokinesis. Mol Cell Biol 32, 1396–1407.

Angulo S, Morales A, Danese S, Llacuna L, Masamunt MC, Pultz N, Cifone MG, De Simone C, Delgado S, Vila J, *et al.* (2011). Probiotic sonicates selectively induce mucosal immune cells apoptosis through ceramide generation via neutral sphingomyelinase. PLoS One 6, e16953.
Badizadegan K, Wheeler HE, Fujinaga Y, Lencer WI (2004). Trafficking of cholera toxin-ganglioside GM1 complex into Golgi and induction of toxicity depend on actin cytoskeleton. Am J Physiol Cell Physiol 287, C1453–C1462.
Bajaj V, Hwang C, Lee CA (1995). hilA is a novel ompR/toxR family member that activates the expression of Salmonella typhimurium invasion genes. Mol Microbiol 18, 715–727.
Bretscher A (1991). Microfilament structure and function in the cortical cytoskeleton. Annu Rev Cell Biol 7, 337–374.
Bretscher A (1999). Regulation of cortical structure by the ezrin-radixin-moesin protein family. Curr Opin Cell Biol 11, 109–116.
Bretscher A, Edwards K, Fehon RG (2002). ERM proteins and merlin: integrators at the cell cortex. Nat Rev Mol Cell Biol 3, 586–599.
Chapman H, Ramstrom C, Korhonen L, Laine M, Wann KT, Lindholm D, Pasternack M, Tornquist K (2005). Downregulation of the HERG (KCNH2) K(+) channel by ceramide: evidence for ubiquitin-mediated lysosomal degradation. J Cell Sci 118, 5325–5334.
Chik CL, Li B, Karpinski E, Ho AK (2001). Ceramide inhibits the outward potassium current in rat pinealocytes. J Neurochem 79, 339–348.
Clarke CJ, Snook CF, Tani M, Matmati N, Marchesini N, Hannun YA (2006). The extended family of neutral sphingomyelinases. Biochemistry 45, 11247–11256.
Criss AK, Ahlgren DM, Jou TS, McCormick BA, Casanova JE (2001). The GTPase Rac1 selectively regulates Salmonella invasion at the apical plasma membrane of polarized epithelial cells. J Cell Sci 114, 1331–1341.
Devaux PF, Morris R (2004). Transmembrane asymmetry and lateral domains in biological membranes. Traffic 5, 241–246.
Eierhoff T, Bastian B, Thuenauer R, Madl J, Audfray A, Aigal S, Juillot S, Rydell GE, Muller S, de Bentzmann S, *et al.* (2014). A lipid zipper triggers bacterial invasion. Proc Natl Acad Sci USA 111, 12895–12900.
Ella KM, Qi C, Dolan JW, Thompson RP, Meier KE (1997). Characterization of a sphingomyelinase activity in Saccharomyces cerevisiae. Arch Biochem Biophys 340, 101–110.
Feltis BA, Wiesner SM, Kim AS, Erlandsen SL, Lyerly DL, Wilkins TD, Wells CL (2000). Clostridium difficile toxins A and B can alter epithelial permeability and promote bacterial paracellular migration through HT-29 enterocytes. Shock 14, 629–634.
Finlay BB, Ruschkowski S, Dedhar S (1991). Cytoskeletal rearrangements accompanying salmonella entry into epithelial cells. J Cell Sci 99, 283–296.
Gilbert RJ, Kramer JM (1984). Bacillus cereus enterotoxins: present status. Biochem Soc Trans 12, 198–200.
Gonzalez-Zorn B, Dominguez-Bernal G, Suarez M, Ripio MT, Vega Y, Novella S, Vazquez-Boland JA (1999). The smcL gene of Listeria ivanovii encodes a sphingomyelinase C that mediates bacterial escape from the phagocytic vacuole. Mol Microbiol 33, 510–523.
Gowrishankar K, Ghosh S, Saha SCR, Mayor S, Rao M (2015). Active remodeling of cortical actin regulates spatiotemporal organization of cell surface molecules. Cell 149, 1353–1367.
Grassme H, Jendrossek V, Riehle A, von Kurthy G, Berger J, Schwarz H, Weller M, Kolesnick R, Gulbins E (2003). Host defense against Pseudomonas aeruginosa requires ceramide-rich membrane rafts. Nat Med 9, 322–330.
Gri G, Molon B, Manes S, Pozzan T, Viola A (2004). The inner side of T cell lipid rafts. Immunol Lett 94, 247–252.
Gulbins E, Dreschers S, Wilker B, Grassme H (2004). Ceramide, membrane rafts and infections. J Mol Med 82, 357–363.
Gulbins E, Szabo I, Baltzer K, Lang F (1997). Ceramide-induced inhibition of T lymphocyte voltage-gated potassium channel is mediated by tyrosine kinases. Proc Natl Acad Sci USA 94, 7661–7666.
Hannun YA (1994). The sphingomyelin cycle and the second messenger function of ceramide. J Biol Chem 269, 3125–3128.
Hecht G, Pothoulakis C, LaMont JT, Madara JL (1988). Clostridium difficile toxin A perturbs cytoskeletal structure and tight junction permeability of cultured human intestinal epithelial monolayers. J Clin Invest 82, 1516–1524.
Hilpela P, Vartiainen MK, Lappalainen P (2004). Regulation of the actin cytoskeleton by PI(4,5)P2 and PI(3,4,5)P3. Curr Top Microbiol Immunol 282, 117–163.
Ho HY, Rohatgi R, Lebensohn AM, Le M, Li J, Gygi SP, Kirschner MW (2004). Toca-1 mediates Cdc42-dependent actin nucleation by activating the N-WASP-WIP complex. Cell 118, 203–216.
Hueck CJ, Hantman MJ, Bajaj V, Johnston C, Lee CA, Miller SI (1995). Salmonella typhimurium secreted invasion determinants are homologous to Shigella Ipa proteins. Mol Microbiol 18, 479–490.
Ito Y, Sato S, Ohashi T, Nakayama S, Shimokata K, Kume H (2004). Reduction of airway anion secretion via CFTR in sphingomyelin pathway. Biochem Biophys Res Commun 324, 901–908.
Ivanov AI, McCall IC, Parkos CA, Nusrat A (2004). Role for actin filament turnover and a myosin II motor in cytoskeleton-driven disassembly of the epithelial apical junctional complex. Mol Biol Cell 15, 2639–2651.
Just I, Selzer J, von Eichel-Streiber C, Aktories K (1995). The low molecular mass GTP-binding protein Rho is affected by toxin A from Clostridium difficile. J Clin Invest 95, 1026–1031.
Kiyokawa E, Baba T, Otsuka N, Makino A, Ohno S, Kobayashi T (2005). Spatial and functional heterogeneity of sphingolipid-rich membrane domains. J Biol Chem 280, 24072–24084.
Knutton S, Baldwin T, Williams PH, McNeish AS (1989). Actin accumulation at sites of bacterial adhesion to tissue culture cells: basis of a new diagnostic test for enteropathogenic and enterohemorrhagic Escherichia coli. Infect Immun 57, 1290–1298.
Lencer WI, Moe S, Rufo PA, Madara JL (1995). Transcytosis of cholera toxin subunits across model human intestinal epithelia. Proc Natl Acad Sci USA 92, 10094–10098.
Lepple-Wienhues A, Belka C, Laun T, Jekle A, Walter B, Wieland U, Welz M, Heil L, Kun J, Busch G, *et al.* (1999). Stimulation of CD95 (Fas) blocks T lymphocyte calcium channels through sphingomyelinase and sphingolipids. Proc Natl Acad Sci USA 96, 13795–13800.
Lingwood D, Simons K (2010). Lipid rafts as a membrane-organizing principle. Science 327, 46–50.
Liu Y, Casey L, Pike LJ (1998). Compartmentalization of phosphatidylinositol 4,5-bisphosphate in low-density membrane domains in the absence of caveolin. Biochem Biophys Res Commun 245, 684–690.
Madara JL, Stafford J, Barenberg D, Carlson S (1988). Functional coupling of tight junctions and microfilaments in T84 monolayers. Am J Physiol 254, G416–G423.
Madara JL, Stafford J, Dharmsathaphorn K, Carlson S (1987). Structural analysis of a human intestinal epithelial cell line. Gastroenterology 92, 1133–1145.
Megha , London E (2004). Ceramide selectively displaces cholesterol from ordered lipid domains (rafts): implications for lipid raft structure and function. J Biol Chem 279, 9997–10004.
Merrill AH Jr, Schmelz EM, Dillehay DL, Spiegel S, Shayman JA, Schroeder JJ, Riley RT, Voss KA, Wang E (1997). Sphingolipids—the enigmatic lipid class: biochemistry, physiology, and pathophysiology. Toxicol Appl Pharmacol 142, 208–225.
Nusrat A, Delp C, Madara JL (1992). Intestinal epithelial restitution. Characterization of a cell culture model and mapping of cytoskeletal elements in migrating cells. J Clin Invest 89, 1501–1511.
Nusrat A, Giry M, Turner JR, Colgan SP, Parkos CA, Carnes D, Lemichez E, Boquet P, Madara JL (1995). Rho protein regulates tight junctions and perijunctional actin organization in polarized epithelia. Proc Natl Acad Sci USA 92, 10629–10633.
Pagano RE, Martin OC, Kang HC, Haugland RP (1991). A novel fluorescent ceramide analogue for studying membrane traffic in animal cells: accumulation at the Golgi apparatus results in altered spectral properties of the sphingolipid precursor. J Cell Biol 113, 1267–1279.
Patel AH, Nowlan P, Weavers ED, Foster T (1987). Virulence of protein A-deficient and alpha-toxin-deficient mutants of Staphylococcus aureus isolated by allele replacement. Infect Immun 55, 3103–3110.
Pelkmans L, Puntener D, Helenius A (2002). Local actin polymerization and dynamin recruitment in SV40-induced internalization of caveolae. Science 292, 535–539.
Pike LJ, Miller JM (1998). Cholesterol depletion delocalizes phosphatidylinositol bisphosphate and inhibits hormone-stimulated phosphatidylinositol turnover. J Biol Chem 273, 22298–22304.
Riegler M, Sedivy R, Sogukoglu T, Castagliuolo I, Pothoulakis C, Cosentini E, Bischof G, Hamilton G, Teleky B, Feil W, *et al.* (1997). Epidermal growth factor attenuates Clostridium difficile toxin A- and B-induced damage of human colonic mucosa. Am J Physiol 273, G1014–G1022.
Romer W, Pontani LL, Sorre B, Rentero C, Berland L, Chambon V, Lamaze C, Bassereau P, Sykes C, Gaus K, Johannes L (2010). Actin dynamics drive membrane reorganization and scission in clathrin-independent endocytosis. Cell 140, 540–553.
Saotome I, Curto M, McClatchey AI (2004). Ezrin is essential for epithelial organization and villus morphogenesis in the developing intestine. Dev Cell 6, 855–864.

Saslowsky DE, Lencer WI (2008). Conversion of apical plasma membrane sphingomyelin to ceramide attenuates the intoxication of host cells by cholera toxin. Cell Microbiol 10, 67–80.

Saslowsky DE, Tanaka N, Reddy KP, Lencer WI (2009). Ceramide activates JNK to inhibit a cAMP-gated K+ conductance and Cl^- secretion in intestinal epithelia. FASEB J 23, 259–270.

Saslowsky DE, te Welscher YM, Chinnapen DJ, Wagner JS, Wan J, Kern E, Lencer WI (2013). Ganglioside GM1-mediated transcytosis of cholera toxin bypasses the retrograde pathway and depends on the structure of the ceramide domain. J Biol Chem 288, 25804–25809.

Si JM, Yu YC, Fan YJ, Chen SJ (2004). Intestinal microecology and quality of life in irritable bowel syndrome patients. World J Gastroenterol 10, 1802–1805.

Simons K, Ikonen E (1997). Functional rafts in cell membranes. Nature 387, 569–572.

Simons K, van Meer G (1988). Lipid sorting in epithelial cells. Biochemistry 27, 6197–6202.

Sot J, Ibarguren M, Busto JV, Montes LR, Goni FM, Alonso A (2008). Cholesterol displacement by ceramide in sphingomyelin-containing liquid-ordered domains, and generation of gel regions in giant lipidic vesicles. FEBS Lett 582, 3230–3236.

Subbaiah PV, Billington SJ, Jost BH, Songer JG, Lange Y (2003). Sphingomyelinase D, a novel probe for cellular sphingomyelin: effects on cholesterol homeostasis in human skin fibroblasts. J Lipid Res 44, 1574–1580.

Taniguchi Y, Ohba T, Miyata H, Ohki K (2006). Rapid phase change of lipid microdomains in giant vesicles induced by conversion of sphingomyelin to ceramide. Biochim Biophys Acta 1758, 145–153.

Tilney LG, Portnoy DA (1989). Actin filaments and the growth, movement, and spread of the intracellular bacterial parasite, Listeria monocytogenes. J Cell Biol 109, 1597–1608.

Vazquez-Boland JA, Kuhn M, Berche P, Chakraborty T, Dominguez-Bernal G, Goebel W, Gonzalez-Zorn B, Wehland J, Kreft J (2001). Listeria pathogenesis and molecular virulence determinants. Clin Microbiol Rev 14, 584–640.

Villalba M, Bi K, Rodriguez F, Tanaka Y, Schoenberger S, Altman A (2001). Vav1/Rac-dependent actin cytoskeleton reorganization is required for lipid raft clustering in T cells. J Cell Biol 155, 331–338.

Walsh SV, Hopkins AM, Chen J, Narumiya S, Parkos CA, Nusrat A (2001). Rho kinase regulates tight junction function and is necessary for tight junction assembly in polarized intestinal epithelia. Gastroenterology 121, 566–579.

Wolf AA, Fujinaga Y, Lencer WI (2002). Uncoupling of the cholera toxin-G(M1) ganglioside receptor complex from endocytosis, retrograde Golgi trafficking, and downstream signal transduction by depletion of membrane cholesterol. J Biol Chem 277, 16249–16256.

Zeidan YH, Jenkins RW, Hannun YA (2008). Remodeling of cellular cytoskeleton by the acid sphingomyelinase/ceramide pathway. J Cell Biol 181, 335–350.